AWARD NUMBER: W81WXWH-14-1-0502

TITLE: Smart Sensing and Dynamic Fitting for Enhanced Comfort and Performance of Prosthetics

PRINCIPAL INVESTIGATOR: Haiying Huang

CONTRACTING ORGANIZATION: University of Texas Arlington
Arlington, TX 76019

REPORT DATE: October 2015

TYPE OF REPORT: Annual

PREPARED FOR: U.S. Army Medical Research and Materiel Command
Fort Detrick, Maryland 21702-5012

REPORT DOCUMENTATION PAGE

Form Approved
OMB No. 0704-0188

1. REPORT DATE	2. REPORT TYPE	3. DATES COVERED
October 2015	Annual	30 Sep 2014-29Sep 2015

4. TITLE AND SUBTITLE

Smart Sensing and Dynamic Fitting for Enhanced Comfort and Performance of Prosthetics

5a. CONTRACT NUMBER

5b. GRANT NUMBER
W81WXWH-14-1-0502

5c. PROGRAM ELEMENT NUMBER

6. AUTHOR(S)

Haiying Huang

E-Mail: huang@uta.edu

5d. PROJECT NUMBER

5e. TASK NUMBER

5f. WORK UNIT NUMBER

7. PERFORMING ORGANIZATION NAME(S) AND ADDRESS(ES)

University of Texas Arlington
500 W. First Street, WH211
Arlington, TX 76019

8. PERFORMING ORGANIZATION REPORT NUMBER

9. SPONSORING / MONITORING AGENCY NAME(S) AND ADDRESS(ES)

U.S. Army Medical Research and Materiel Command
Fort Detrick, Maryland 21702-5012

10. SPONSOR/MONITOR'S ACRONYM(S)

11. SPONSOR/MONITOR'S REPORT NUMBER(S)

12. DISTRIBUTION / AVAILABILITY STATEMENT

Approved for Public Release; Distribution Unlimited

13. SUPPLEMENTARY NOTES

14. ABSTRACT

The objective of the project is to enhance the long-term fit and performance of prosthetic sockets through smart sensing, adaptive interface, and shear-based dynamic fitting strategy. In the first year, we focused on developing the antenna pressure/shear sensors and the bubble actuators for pressure regulation. An antenna sensor that is capable of measuring shear and pressure displacements simultaneously was designed, fabricated, and validated. Three different test fixtures and associated control software were developed for sensor calibration. Fabrication techniques were developed for implementing flexible sensors on commercial prosthetic liner or custom made liner materials. We have characterized the load bearing capability of bubble actuator arrays at different actuation pressures. A "limb-socket" laboratory test setup was developed for capturing the internal pressure change of bubble actuators when the "limb" was subjected to the external force.

15. SUBJECT TERMS

Prosthetic socket, shear/pressure sensor, active interface, bubble actuator

16. SECURITY CLASSIFICATION OF:			17. LIMITATION OF ABSTRACT	18. NUMBER OF PAGES	19a. NAME OF RESPONSIBLE PERSON
a. REPORT	b. ABSTRACT	c. THIS PAGE			USAMRMC
Unclassified	Unclassified	Unclassified	Unclassified	25	19b. TELEPHONE NUMBER *(include area code)*

Contents

1 INTRODUCTION

The objective of the project is to enhance the long-term fit and performance of prosthetic sockets through smart sensing, adaptive interface, and shear-based dynamic fitting strategy. In the first year, we focused on developing the antenna pressure/shear sensors and the bubble actuators for pressure regulation. An antenna sensor that is capable of measuring shear and pressure displacements simultaneously was designed, fabricated, and validated. Three different test fixtures and associated control software were developed for sensor calibration. Fabrication techniques were developed for implementing flexible sensors on commercial prosthetic liner or custom made liner materials. We have characterized the load bearing capability of bubble actuator arrays at different actuation pressures. A "limb-socket" laboratory test setup was developed for capturing the internal pressure change of bubble actuators when the "limb" was subjected to the external force.

2 KEYWORDS

Prosthetic socket, shear/pressure sensor, antenna sensor, active interface, bubble actuator

3 ACCOMPLISHMENTS

· **What were the major goals of the project?**

The three aims of the projects are: 1) Demonstrating real-time measurements of interfacial stresses and residual limb volume; 2) Producing active interfaces that can automatically adjust the fitting of the prosthetic socket; 3) Testing the active prosthetic interface and the shear-based fitting strategy in clinical settings.

First year milestones:

- *Author manuscript that demonstrates simultaneous measurement of shear and pressure stresses (by July 2015) – experiment is completed. Manuscript preparation under way.*
- *(Added) Demonstrate sensor implementation on prosthetic liner materials - completed*
- *Demonstrate a laboratory prototype that can dynamically change pressure profile (by September 2015) – 90% completed*
- *(postponed) Author manuscript that demonstrates volume and bio-impedance sensing using antenna sensors (Expected completion date: September 2016)*

· **What was accomplished under these goals?**

Accomplishment #1: Demonstrated simultaneous shear and pressure sensing using antenna sensors implemented on commercial prosthetic liner materials

· **Specific objective:** 1) realize antenna sensors that can be implemented on prosthetic liners and can simultaneously measure shear and pressure; 2) develop test fixture for characterizing the sensor performance.

· **Major activities**:

1) Design and fabricate the shear/pressure sensor: as shown in Figure 1(a), the sensor consists of a patch antenna and a U-shaped reflector separated from the patch antenna by the liner material. Pressure changes the vertical position of the reflector while shear changes the lateral position of the reflector slot. The effects of the shear and pressure on the antenna frequencies were first validated by developing a numerical simulation model (See Figure 1(b)). The patch antenna and the U-shaped reflector, fabricated on commercial dielectric substrate, are shown in Figure 1(c). The antenna radiation patch has a length of 12.75 mm and a width of 11.25 mm. The U-shaped reflector has a total length of 35 mm and a total width of 25 mm. The slot width is 5 mm.

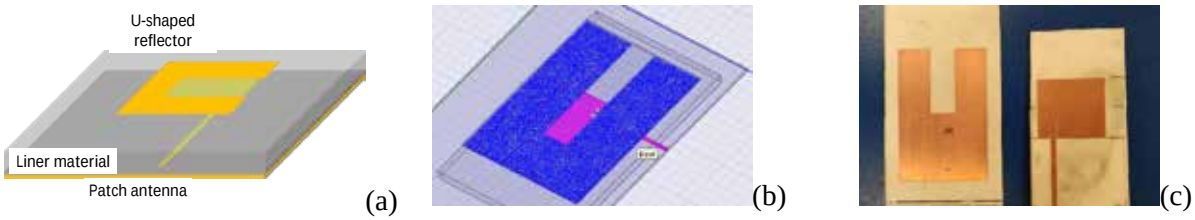

Figure 1: Antenna shear/pressure sensor; (a) sensor configuration; (b) numerical simulation model; (c) sensor components fabricated on commerical substrate.

2) Implement test fixtures for sensor characterization: three test fixtures were implemented for characterizing the sensor performance. Test fixture #1, shown in Figure 2(a), was implemented to apply shear and pressure displacements independently so that the numerical simulation can be validated. The test fixture was automated using two motorized translation stages. During the experiment, the position of the patch antenna was fixed while the position of the reflector was translated laterally and vertically using the two motorized translation stages. Test fixture #2, shown in Figure 2(b), includes an outer cylinder imitating the prosthetic socket and an inner cylinder imitating the residual limb. The outer cylinder is equipped with two air bubbles that apply pressures to the sensor packages. Shear forces were applied by pushing the inner cylinder downward using a mechanical tester. Two 3D printed sensor packages were mounted on the inner cylinder. Test fixture #3, as shown in Figure 2(c), enables characterizing the sensors implemented on soft prosthetic liners. The sensor package is sandwiched between two movable plates. One movable plate is mounted under a load cell while the other one is mounted above the air bubble. Increasing the pressure of the air bubble compresses the sensor package, which in turn pushes the upper plate against the load cell. The pressure displacement of the sensor package is measured by a LVDT mounted on the top plate. A patch antenna covered with a 5 mm thick prosthetic liner is shown in Figure 2(d). The U-reflector was glued on a flat plate; it was placed on top of the prosthetic liner and its position can be adjusted by the shear applying rod shown in Figure 2(c). The rod was pushed using a translation stage actuated by a manual micrometer. The lateral position of the reflector plate was measured using a LVDT sensor mounted on the side of the test fixture.

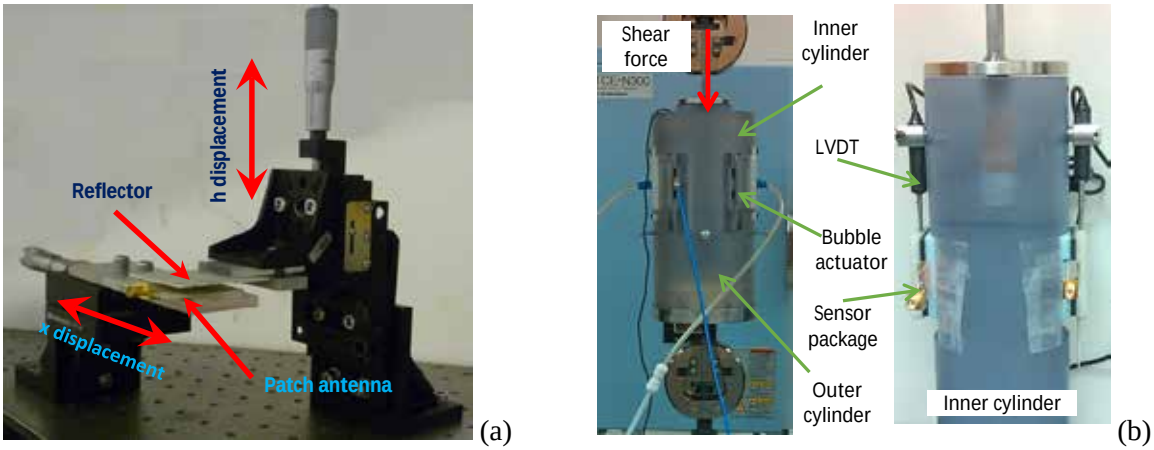

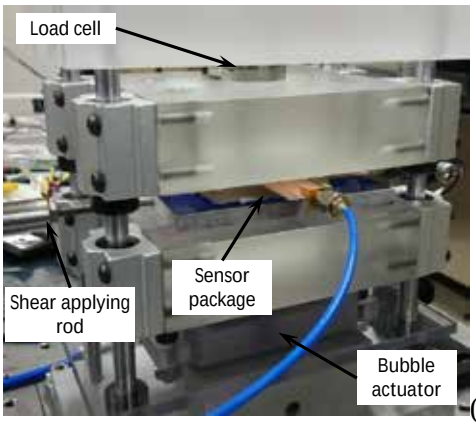

(b)

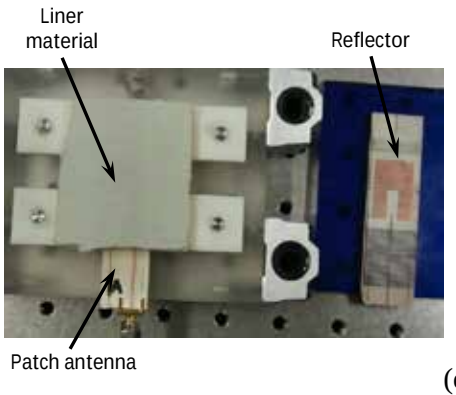

(d)

Figure 2: test fixtures for sensor characterization; (a) test fixture #1 for validating numerical simulation; (b) test fixture #2 immitate prosthetic socket and residula limb; (c) test fixture #3 for testing sensors implemented on liner materials; (d) sensor package implemented using liner materials.

3) *Develop data processing algorithm for inversely determining the shear and pressure displacements from the measured antenna frequencies*: the measurement data were first curve fitted using two-variate polynomials. The shear and pressure displacements of the sensor were then inversely determined from the measured antenna resonant frequencies. The derived displacements were compared with the actual displacement inputs to determine the measurement accuracy of the sensor. The algorithm was implemented in MATLAB.

· **Significant results:** the measured antenna resonant frequencies under different combinations of shear and pressure displacements are shown in Figure 3. The measurement data were curve fitted using second-order multivariate polynomials, i.e. $f = P_{00} + P_{10}*x + P_{01}*y + P_{20}*x^2 + P_{11}*x*y + P_{02}*y^2$. An R^2 value of 0.9979 was achieved for the f_{01} frequency while the R^2 value for the f_{10} frequency is 0.9980.

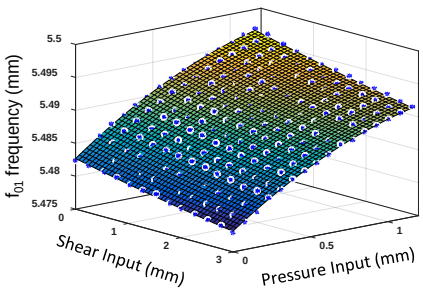

(a)

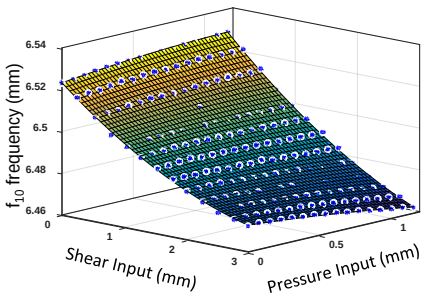

(b)

Figure 3: measured antenna resonant frequencies as a function of the shear and pressure displacement inputs; (a) f_{01} antenna frequency; (b) f_{10} antenna frequency.

The differences between the shear and pressure displacements inversely determined from the measured antenna resonant frequencies and the actual shear and pressure inputs are shown in Figure 4. The total pressure displacement was 1.2 mm and the total shear displacement was 3 mm. The errors between the measured displacements and the actual inputs are within ±0.1 mm for the pressure displacements and within ±0.15 mm for the shear displacements, corresponding to ±8% for the pressure and ±5% for the shear displacements. Some of these errors may be contributed by the LVDT sensors, which have measurement uncertainties of around 0.06 mm.

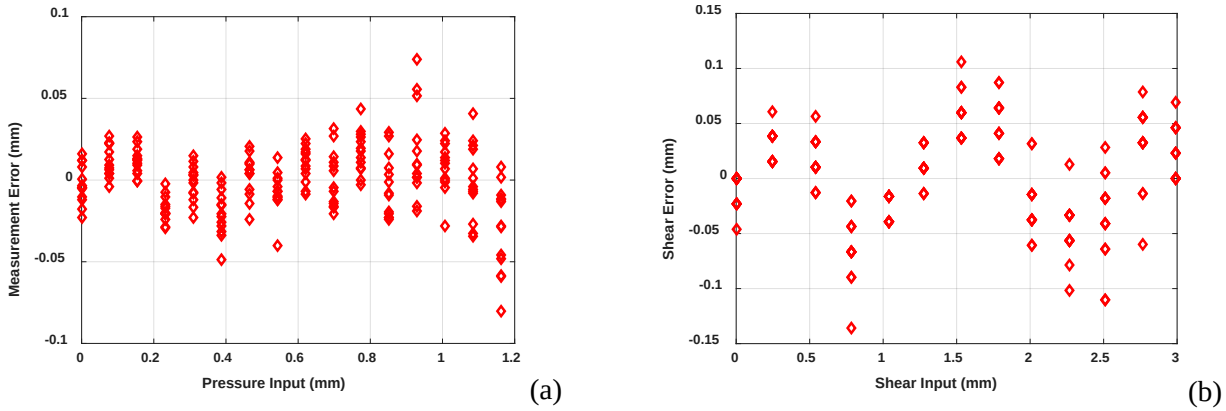

(a) (b)

Figure 4: Differences between the displacements inversely determined from the measured frequencies and the actual displacement inputs; (a) pressure displacements; (b) shear displacements.

Accomplishment #2: Established fabrication techniques to either embed shear/ pressure antenna sensors in custom-made liners or integrate shear/ pressure antenna sensors with commercial liners

· **Specific objectives:** demonstrate flexible shear/ pressure antenna sensors with the liner material as its superstrate

· **Major activities:**

1) Developed numerical simulation model for designing the shear/ pressure antenna sensors with the linear material as its superstrate (See Figure 5(a));

2) *Fabricated customized liners with comparable hardness as that of commercial prosthetic liners*: as shown in Figure 5(b), the silicone rubber was casted on top of the patch antenna using a custom designed mold. A thickness of 5 mm was first casted and the U-shaped reflector was placed on the top surface of the cured silicone rubber. A thin layer with a thickness of 1mm was subsequently casted on the reflector. This approach enables the placement of the reflector at selected distance from the patch antenna. The resulting sensors are stable, flexible and can be mounted on the human body.

3) *Investigated different adhesive materials for bonding the patch antenna and reflector to commercial prosthetic liners*: we discovered that most adhesive will not bond well with the commercial prosthetic liner. Medical Adhesive is the only product that works, even though the cured bonding layer is still a little stiffer than the liner. A shear/pressure sensor was realized by fabricating the patch antenna and the reflector using a flexible electrical substrate material and bonding these two components on the prosthetic liner using medical adhesive (see Figure 5(c)).

4) Validated the radiation properties of shear/pressure antenna sensors embedded in silicon rubber material or bonded on commercial liners.

· **Significant results:** The return losses of the patch antenna without and with the superstrate are compared in Figure 6. For the sensor bonded on the commercial liner, the simulation predicts that the S11 parameters of shear/ pressure antenna sensor will shift to the left after the liner material is placed on top of the patch antenna. This prediction was validated by the measurement results, as shown in Figure 6(a). Since the dielectric constant of the liner material was not known, this parameter was adjusted in the simulation model to achieve a reasonable match between the simulation and measurement results. The fabrication uncertainty, such as the soldering of the SMA connector, could also contribute to these discrepancies. Nonetheless, both the simulation and measurements indicate that the patch antenna maintain its radiation characteristics with the superstrate and the reflector placed on top of it.

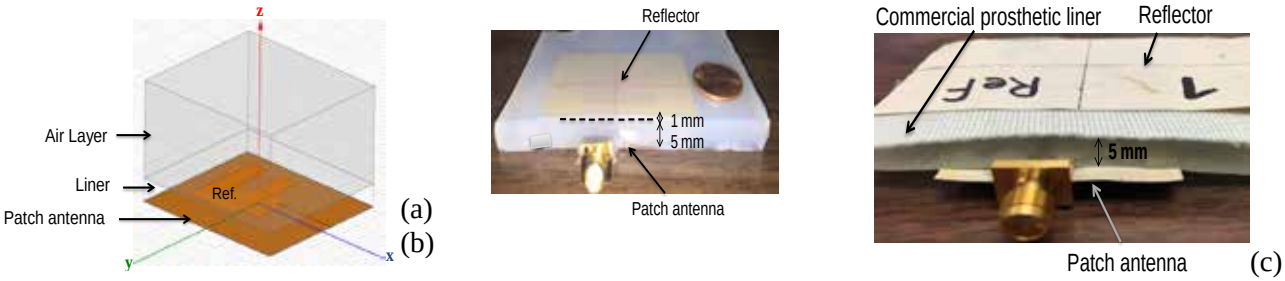

Figure 5: shear/ pressure antenna sensor implemented with soft liner materials as superstrate; (a) numerical simulation model; (b) flexible patch antenna embedded in 5 mm thick RTV silicon rubber; (c) shear/ pressure antenna sensor bonded on the standard 5mm thick commercial liner.

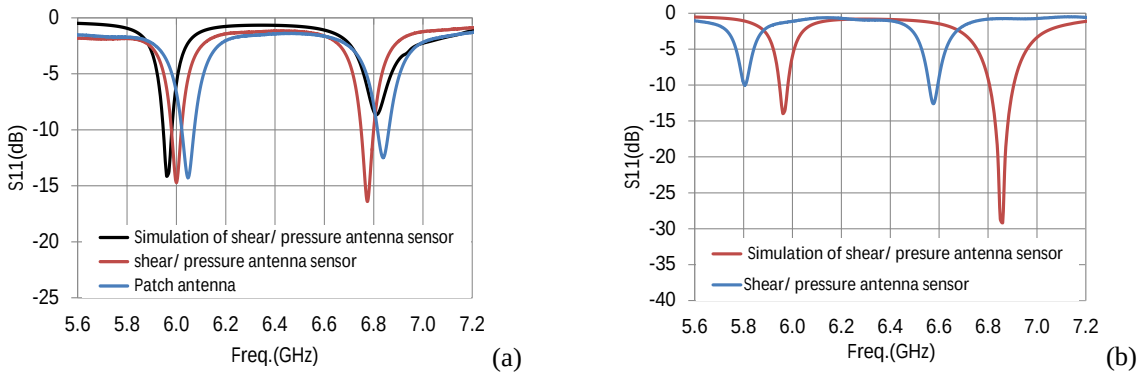

Figure 6: comparison between the measured and simulated scattering parameters; (a) shear/ pressure antenna sensor bonded on commercial liner; (b) shear/ pressure antenna sensor embedded in the custom-made liner.

Accomplishment #3: Fabricated the shear/ pressure antenna sensors from conductive fabrics/ foams

· **Specific objectives:** Develop sensors that are more flexibility and compatibility with human skin

· **Major Activities:**

1) *Explored flexible conductive materials to serve as electrode materials for the antenna sensor*: we found that both conductive foam and conductive fabric can serve as the electrode materials for the antenna sensor. These materials are much more flexible, stretchable, and breathable than copper films and thus are more suitable for the prosthetic applications.

2) *Fabricate flexible antenna sensors using conductive foam*: the antenna radiation patch, the ground plane, and the reflectors can be cut from the conductive foams using laser machining. The patch antenna can then be assembled by bonding the conductive foam patterns on flexible substrate (See Figure 7(a)) or Kapton (see Figure 7(b)). As shown in Figure 7(c), the resulting patch antenna sensor is very flexible and can be easily bend.

· **Significant results:** shear/ pressure antenna sensors were fabricated by bonding the patch antenna and reflector on commercial prosthetic liner (see Figure 8(a)). The S11 curve of the fabricated antenna sensor is shown in Figure 8(b), which shows that the antenna sensor fabricated from the conductive foam has a satisfactory resonant response.

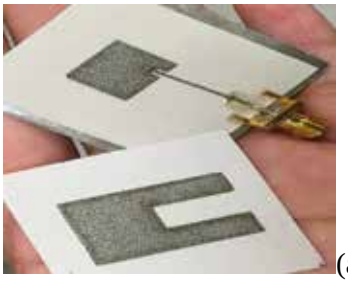
(a)
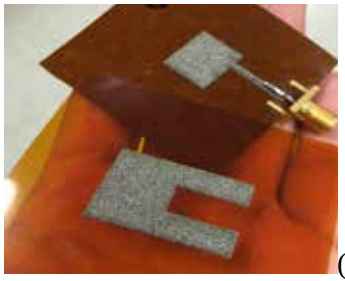
(b)

(c)

Figure 7: implementing flexible sensor using conductive foam; (a) antenna and reflector bonded on flexible dielectric material; (b) antenna and reflector bonded on Kapton; (c) flexibility of antenna fabricated from conductive foam and Kapton.


(a)
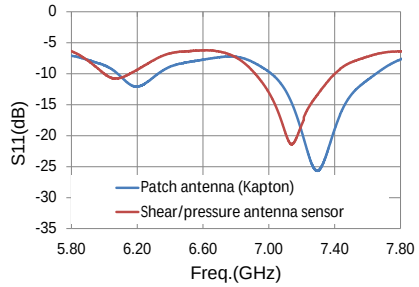

(b)

Figure 8: (a) shear/pressure sensor fabricated on flexible dielectric and conductive materials; (b) measured S11 curves of fabricated sensor.

*Accomplishment #4***:** Developed fabrication techniques for embedding the shear/ pressure antenna sensors in custom-made prosthetic liners

- **Specific objectives:** demonstrate the shear/ pressure antenna sensor on curved surfaces;
- **Major Activities:**

1) Surveyed literature to find the best way for make custom prosthetic liners and identified casting as suitable method among dipping and injection methods;
2) Designed and manufactured a small mold using 3-D printing techniques for embedding antenna sensors in custom-made liners (See Figure 9(a));
3) Fabricated part of prosthetic liner ring using silicone material and compare its hardness with that of commercial prosthetic liners (See Figure 9(b));
4) Implemented one patch antenna sensor in RTV silicone material using the mold (See Figure 9(c))

- **Significant results:** Realize antenna shear and pressure sensor on prosthetic liners (see Figure 9(c))


(a)

(b)
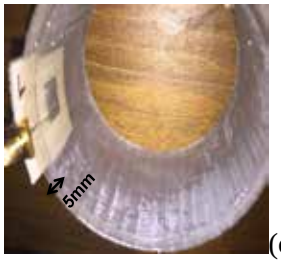

(c)

Figure 9: Fabricate shear/ pressure antenna sensor on curved surface; (a) 3D printed casting mold; (b) fabricated custom-made liner by casting method; (c) a patch antenna sensor embedded with the curved surface custom-made liner.

Accomplishment #5: Characterized the load bearing capability of bubble actuator arrays at different actuation pressures

· **Specific objectives:** 1) investigate different test setups for load-displacement measurements; 2) validate the load bearing capability of the single bubble actuator and bubble actuator array.

· **Major activities**:

1) Developed the simulation model for investigating the external force-displacement relationship of the bubble actuators under different actuation pressures by comparing and validate the model with the experimental results (see Figure 10(a));
2) Measured the displacement of a single bubble actuator and bubble actuator array under different actuation pressures when subjected to external normal forces of up to 36 N (see Figure 10(b));
3) Recorded the internal pressure change of the single bubble actuator and bubble actuator array with increased external load;

· **Significant results:** Obtained the load-displacement relationship and internal pressure change when applying external force on bubble arrays at different actuation pressures (see Figure 11). These results will provide the insight to the internal pressure control while ensuring the prosthetic fit during walking.

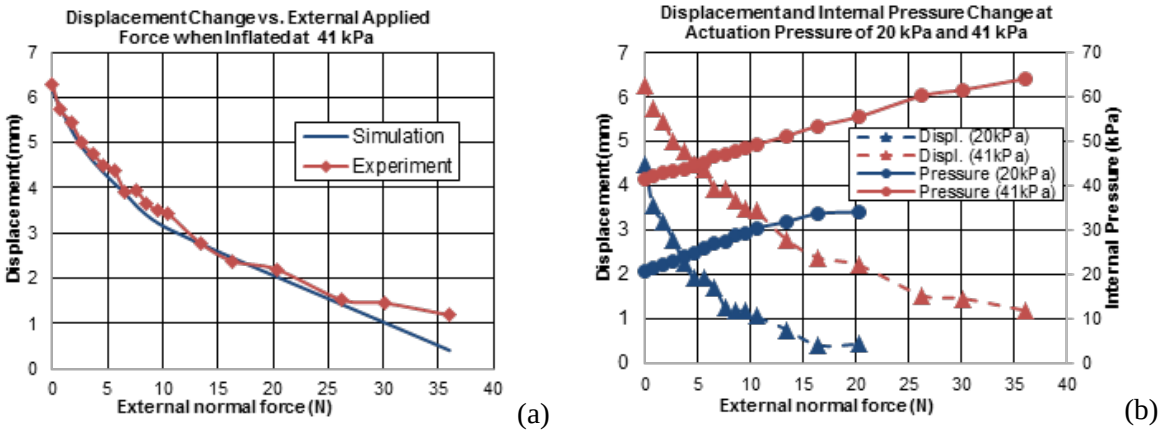

Figure 10: (a) a good agreement between simulation results and displacement measurements of a single RTV-SR bubble actuator; (b) The decrease in displacement and increase in internal pressure of a single bubble actuator when increasing the external force for actuation pressure of 20 kPa and 41 kPa. A single bubble (2cmx3cm) can bear up to 36 N of force without collapsing, which indicates the robustness of the bubble actuators.

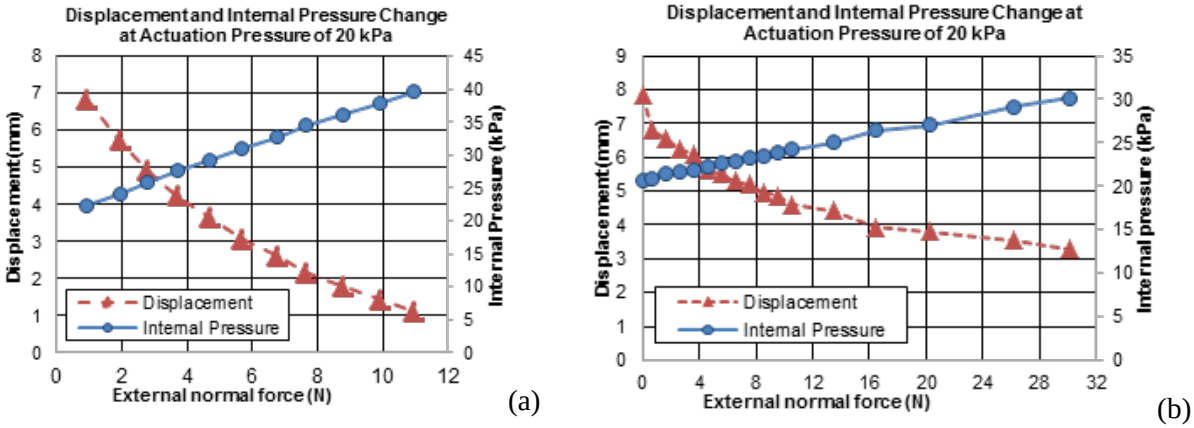

Figure 11: (a) A single PR bubble actuator can bear external force up to 11 N without being compressed to flat; (b) An array of PR bubble actuators (four actuators) can bear up to 30 N with less increase in internal pressure.

Accomplishment #6: Built a "limb-socket" laboratory test setup for capturing internal pressure change of bubble actuators when the "limb" was subjected to the external force

· **Specific objectives:** 1) integrate the internal pressure sensor with bubble actuator arrays and measure internal pressure variations due to the applied external forces; 2) set the pressure range required for dynamic prosthetic fitting application.

· **Major activities**:

1) Manufactured a small size limb-socket test apparatus using 3D printing techniques;
2) Built a laboratory test setup using bubble actuator arrays with integrated internal pressure sensors and an associated load cell to record the internal pressure change and applied force in real-time (see Figure 12);
3) Visited the clinical site and fabricated an anatomically correct prosthetic socket from thermal plastic and a corresponding positive mold to identify the load-tolerant and load-nontolerant areas on the residual limb model.

· **Significant Results:** Developed the data acquisition system to simultaneously record the internal pressure change and the applied load over time. The limb-socket test apparatus will allow us to measure interface pressures and to develop the pressure control capability over load tolerant areas.

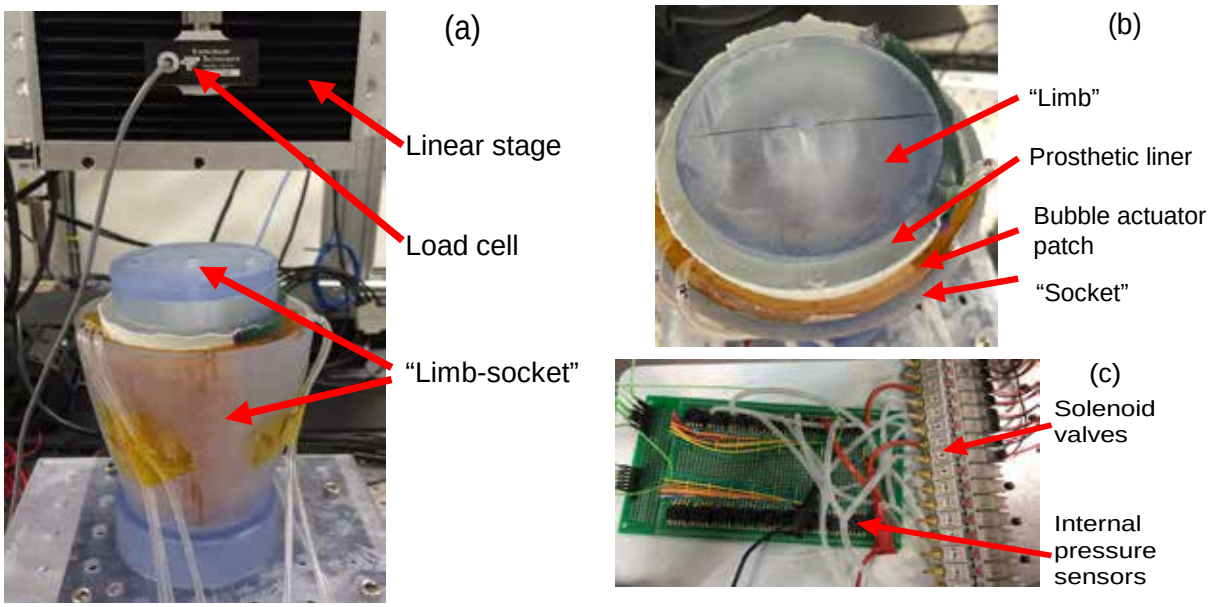

Figure 12: (a) "Limb-socket" test setup; (b) Detailed structure of "limb-socket" test setup; (c) Internal pressure sensor array with associated solenoid valves

Accomplishment #7: Built an anatomically accurate residual limb using silicone rubber and a paired socket by working with Prosthetics and Orthotics lab at UT Southwestern

· **Specific objectives:** 1) Identify the anatomical load tolerant areas and load intolerant areas for transtibial amputees; 2) Refine the shape and size of the bubble actuator patch to match the load tolerant areas; 3) Build a limb-socket setup with integrated bubble actuators to simulate the amputee motion and map the pressure at load tolerant areas during walking.

· **Major activities**:

1) Fabricated a stump using the cast from Prosthetic and Orthotics Lab at UT Southwestern with RTV silicone rubber to imitate the tissue composition, see Figure 13(a);
2) Fabricated a paired socket using thermoplastic in Prosthetic and Orthotics Lab at UT Southwestern;
3) 3D scanned the stump and designed a fixture to build a limb-socket setup for simulating amputee motion;

4) Fabricated bubble actuator patches using RTV silicone rubber in different shapes and sizes to match different load tolerant areas, see Figure 13(b);
5) Attached the bubble actuator patches onto the inner wall of the socket and route all airlines along the socket. Each actuator is individually connected to an in-line pressure sensor (see Figure 13(c)).

· **Significant results:** Built an anatomical accurate limb-socket with integrated bubble actuators at load tolerant areas. The limb-socket setup, as shown in Figure 13(d), will be used to simulate the amputee motion in a laboratory environment and the integrated actuator with in-line pressure sensor will be used to map the pressure at load tolerant areas.

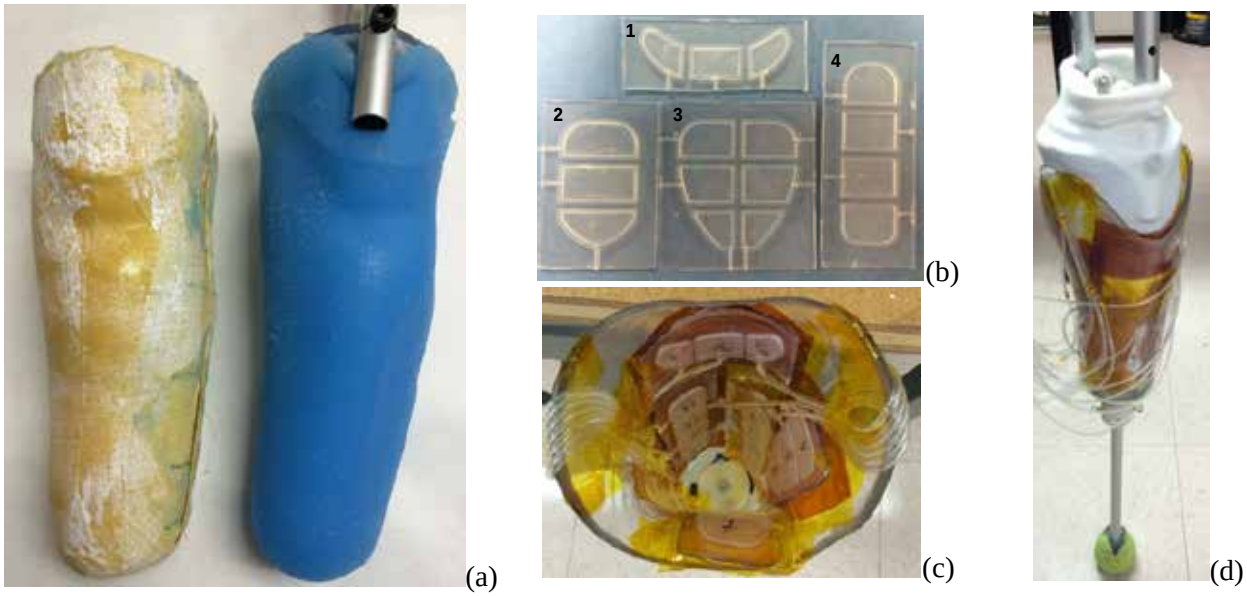

(a) (b) (c) (d)

Figure 13: Limb-socket setup with integrated bubble actuators; (a) fiberglass cast and molded silicone rubber stump; (b) bubble actuator patches made to match different load tolerant areas: #1 is for patellar ligament, #2 is for medial tibial flare, #3 is for posterior compartment, #4 is for medial shaft of tibia, anterior compartment, and lateral shaft of fibula; (c) Socket with integrated bubble actuators at load tolerant areas; (d) limb-socket walking simulator with bubble actuator at the interface

Accomplishment #8: Built a pneumatic control system to actuate multiple bubble actuators with various set pressures using separate air lines each with its own valve and air pressure sensor

· **Specific objectives:** 1) Provide an accurate and responsive means of sensing air pressure within individual bubble sections 2) Control the pressurization of air bubbles using valves and an air pressure regulator

· **Major activities**:

1) Developed and assembled printed circuit boards (PCBs) to mount 24 air pressure sensors and 28 MOSFET switches;
2) Programmed 2 Arduino Uno microcontroller boards with Mayhew Mux Shields to provide 48 digital output and 48 Analog input lines to a MATLAB interface;
3) Fabricated a mounting board for the various components including the air pressure sensor board, MOSFET board, 32 miniature solenoid valves, 2 Arduino microcontrollers, and the associated wires and tubing;
4) Developed a MATLAB graphical user interface (GUI) to help implement an automated inflation scheme to the various bubble patches and regions.

· **Significant results:** Assembled a pneumatic control system to facilitate testing and pressure mapping by integration with MATLAB graphing for data visualization (see Figure 14). This data processing will be used to implement a control system to modulate interface pressures during walking simulation.

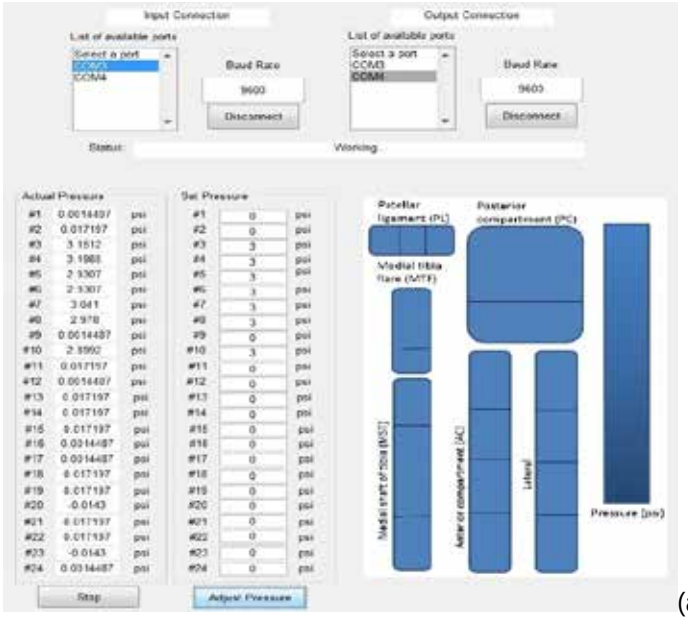

(a)


(c)

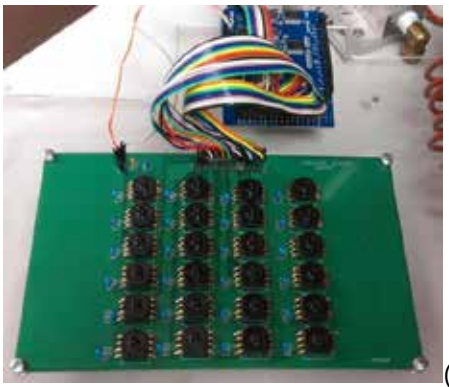
(d)


(e)

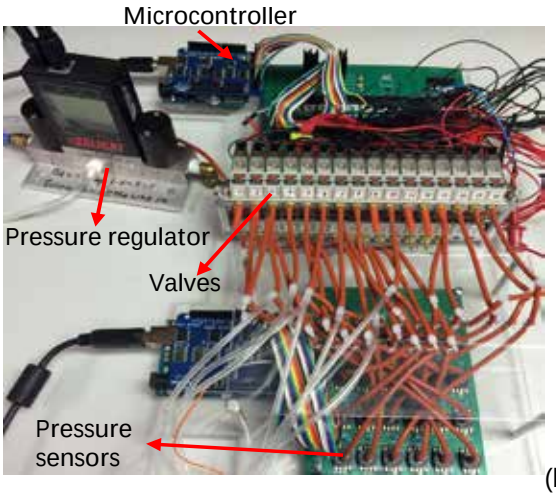

(b)

Figure 14: (a) The GUI showing read and set pressure values; (b) The acrylic mounting board showing various labeled components; (c) The MOSFET board; (d) The pressure sensor board; (e) Solenoid valves

· **What opportunities for training and professional development has the project provided?**

The project supports two graduate students and two research scientists. It offers a unique opportunity for the graduate students, the research scientists and the PIs to interact with medical researchers at UT Southwestern medical school and gain insights and knowledge related to prosthetics and orthopedics.

· **How were the results disseminated to communities of interest?**

The PI presented research results at two conferences, i.e. the SPIE smart materials and structures conference and the annual conference of the biomedical engineering society. The PI also presented the research at UTA College of Engineering Parent Weekend and at a lecture of disability studies as well as discussed the project with representatives from industrial companies, e.g. Flextronics. UTA published a news release on the award of the grant.

· **What do you plan to do during the next reporting period to accomplish the goals?**

1) Characterize the shear/pressure sensor implemented in prosthetic liners using the test fixture imitating the prosthetic socket;
2) Develop portable interrogation system for the antenna sensor;
3) Develop circumference and bio-impedance antenna sensors;
4) Modify the socket with recessed pockets for lower profile bubbles and airline channeling;
5) Measure the internal pressure of bubble arrays during simulated walking load conditions;
6) Modulate actuation pressure based on internal pressure changes while simulating walking.

4 IMPACT

· **What was the impact on the development of the principal discipline(s) of the project?**

The validation of the shear/pressure sensor provides a much-needed sensor technology to advance the smart control of prosthetic socket. These sensors will offer a physics based objective instrument to evaluate the current practices of prosthetic fitting.

The realization of flexible sensors implemented in prosthetic liners will lead to low-cost smart liners that are comfortable to wear on a daily basis.

The studies of the bubble actuator will enable more precise adjustments of the prosthetic fitting at targeted areas.

· **What was the impact on other disciplines**

The sensor and actuator technologies developed in this project can be easily adapted for other applications, such as diabetic foot monitoring, wheelchair cushions, hospital beds, etc.

The flexible antenna sensor can be extended for other wearable devices.

· **What was the impact on technology transfer?**

A full patent is filed (US9138170 B2).

· **What was the impact on society beyond science and technology?**

None to report.

5 CHANGES/PROBLEMS

· **Changes in approach and reasons for change**

The design of the antenna sensor is changed so that one antenna sensor can simultaneously measure shear and pressure, which makes the antenna sensor much simpler. After discussing with the researchers at UT Southwestern Medical School, we decided to explore the implementation of the antenna sensors on the prosthetic liner, which is more practical and require less modification of the prosthetic socket.

· **Actual or anticipated problems or delays and actions or plans to resolve them**

One graduate student resigned and the new student cannot join due to visa problem. The PI is filling in to make up the shortage of human resources. Two more graduate students are recruited and are waiting for their visas to join in spring 2016.

Some of the MOSFETs gate input are not properly grounded and result in non-responsive valves. The MOSFET board requires signal conditioning to ensure reliable valve operation. Voltage regulators for the boards are overheating causing unreliable operation when left on for long periods of time. The power supply requires optimization to increase efficiency and reduce heat.

· **Changes that had a significant impact on expenditures**

Delay in hiring graduate students due to visa issues.

· **Significant changes in use or care of human subjects, vertebrate animals, biohazards, and/or select agents**

None.

6 PRODUCTS

· One conference paper and two conference presentations;
· UTA news release;
· Project description at the PI's website (astl.uta.edu);
· One patent application filed (US9138170 B2);
· Test fixtures for characterizing the antenna sensor and associate control software;
· Flexible antenna shear/pressure sensors implemented on flexible liner materials;
· Techniques for fabricate sensors on customized prosthetic liners;
· An anatomically correct limb-socket test setup for simulating amputee walking;
· Bubble actuator patches made to match the size and shape of load tolerant areas;
· A pneumatic control system for measuring and adjusting internal pressures;
· A user interface allowing for the implementation of automated inflation schemes and display of read pressures across the bubble actuators.

7 PARTICIPANTS & OTHER COLLABORATING ORGANIZATIONS

· **What individuals have worked on the project?**

Name: Haiying Huang
Project Role: PI
Researcher Identifier (e.g. ORCID ID):
Nearest person month worked: 3
Contribution to Project: Advise students and help with data analysis

Name: Farah Ahmed
Project Role: Graduate Research Assistance
Researcher Identifier (e.g. ORCID ID):
Nearest person month worked: 9
Contribution to Project: Characterize 3D printed antenna shear/pressure sensor

Name: Shahnavaz Eilbeigi
Project Role: Graduate Research Assistance
Researcher Identifier (e.g. ORCID ID):
Nearest person month worked: 11
Contribution to Project: Investigate sensor fabrication technique

Name: Muthu Wijesundara
Project Role: Co-PI
Researcher Identifier (e.g. ORCID ID):
Nearest person month worked: 3 (For the first year of the project)
Contribution to Project: Provide the guidance of test setup design and configuration

Name: Wei Carrigan
Project Role: Researcher
Researcher Identifier (e.g. ORCID ID):

Nearest person month worked: 3 (For the first year of the project)
Contribution to Project: Built test setup and performed test and data analysis

Name: Caleb Nothnagle
Project Role: Researcher
Researcher Identifier (e.g. ORCID ID):
Nearest person month worked: 3 (For the first year of the project)
Contribution to Project: Configured test apparatus and performed initial testing

- **Has there been a change in the active other support of the PD/PI(s) or senior/key personnel since the last reporting period?**
  Nothing to Report

- **What other organizations were involved as partners?**
  Organization Name: The Ohio Willow Wood Company
  Location of Organization: Mt. Sterling, Ohio
  Partner's contribution to the project: technical consultant

8 SPECIAL REPORTING REQUIREMENTS

Quad chart (see appendix)

9 APPENDICES

- Quad chart
- SPIE conference paper

Sensing and Dynamic Fitting for Enhanced Comfort and Performance of Prosthetics

OR130167

Award number: W81WXWH-14-1-0502

PI: Haiying Huang **Org:** University of Texas Arlington **Award Amount:** $744,300

Study/Product Aim(s)

- Demonstrate real-time measurements of interface stresses and residual limb volume
- Produce active interfaces that can automatically adjust the fitting of the prosthetic socket
- Test the active prosthetic interface and the shear-based fitting strategy in clinical settings

Approach

We will develop a smart prosthetic interface consisting of two inserts; a sensor insert and an actuator insert. The sensor insert will contain pressure, shear, circumference, and bio-impedance sensors while the actuator insert will be equipped with vacuum suction ports and pressurized bubbles. A shear-based fitting strategy will be implemented to guide the automatic adjustment of the socket. The smart socket will be tested in clinical settings to evaluate the shear-based fitting strategy.

Combined shear/pressure Test

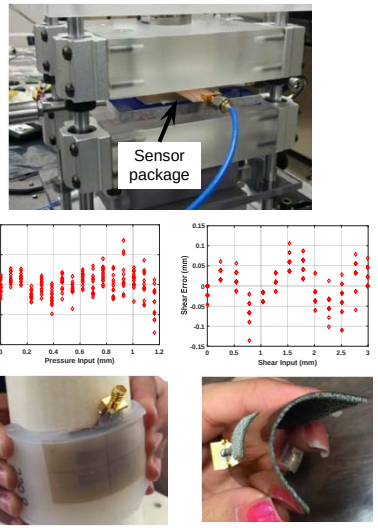

Socket with integrated actuators

Anatomically correct limb-socket setup

Timeline and Cost

Activities CY	14	15	16	17
Characterize sensor performance				
Demonstrate sensor insert				
Produce actuator inset				
Test smart socket in clinical settings				
Estimated Budget ($K)	**$50**	**$250**	**$250**	**$200**

Updated: 10/31/2015

Goals/Milestones

CY14 Goal – demonstrate simultaneous shear and pressure sensing

✓Characterize sensor performance on test bed

✓Design, fabricate, and characterize bubble actuators

CY15 Goals – realize sensor insert and actuator insert

☐Investigate limb volume sensors

☐Realize and characterize sensor insert

✓Realize and characterize actuator insert

CY16 Goal – demonstrate smart socket

☐Validate shear-based fitting strategy

☐Conduct phase I clinical test

CY17 Goal – Conduct phase II clinical test

☐ Improve smart socket for phase II clinical test

Comments/Challenges/Issues/Concerns

- Actual expenditure may not be update due to complications related to accounting system changes

Budget Expenditure to Date

Projected Expenditure: $ 233,780

Actual Expenditure: $203,228

Simultaneous Shear and Pressure Sensing Based on Patch Antenna

Hao Jiang[1], Haiying Huang[2,*]
1 School of Mechanical Science and Engineering, Huazhong University of Science and Technology, 1037 Luoyu Road, Wuhan, Hubei 430074, China
2 Department of Mechanical and Aerospace Engineering, University of Texas at Arlington, 500 W. First Street, WH211, Arlington, TX 76019, USA

ABSTRACT

In this paper, we presented a microstrip patch antenna sensor that is capable to measure the shear and normal deformations simultaneously. The sensor was designed based on the electromagnetic interference between a microstrip patch antenna and a metallic reflector separated by a distance. By placing the reflector on top of the patch antenna, the electromagnetic wave radiated by the patch antenna is reflected by the reflector and interferes with the electromagnetic field of the radiation patch, which in turn changes the antenna resonant frequencies. Since the antenna resonant frequencies are related to the lateral and vertical positions of the metallic reflector, the shear force and normal pressure that shift the reflector laterally and vertically can be detected by monitoring the antenna resonant frequencies. The numerical simulation and experimental measurements were carried out to evaluate the relationship between the antenna resonant frequencies and the shear and normal displacements. A data processing scheme was developed to inversely determine the shear and normal displacements from the antenna resonant frequencies.

Keywords: shear sensor, pressure sensor, microstrip patch antenna sensor, wireless sensor.

1. INTRODUCTION

Mechanical stress applied on a planar surface consists of two components: the pressure acting normal to the surface and shear stress acting tangential to the surface. These interfacial stresses are of great importance for the studies of reactions and properties of the interfaces. Due to the lack of instruments that can measure plantar shear forces reliably, most of the studies were focused on pressure measurements. However, planar shear stresses also play a major role in many applications, such as ulcer formation[1-4], grasping control and slippage detection[5-8] etc.

Since the shear stress is usually coupled with the pressure in many applications, a variety of methods that are capable to measure pressure and shear stress simultaneously were developed in the past decades. These methods can be categorized into strain gauges[12], capacitive sensors[13-15], piezoelectric films[16], and optical methods[17,18], etc. Five sets of strain gauge rosettes were used by Chen et al[12] to measure shear and pressure separately, in which three channels were used for pressure measurements and two were used for shear stress measurements. In a capacitive shear and pressure sensor, one of the capacitor plates was divided into pieces, thus the relative position between the plates can be determined by the measured capacitance from different channels[13-15]. The disadvantages of the capacitive sensors are their susceptibilities to electrical interference and moisture. A pressure and shear sensor based on the piezoelectric effect was reported using a stacked polyvinylidenefluoride material, which consists of four separate sensor elements[16]. Besides multiple channels should be used for data acquisition, the piezoelectric films based sensors are sensitive to temperature changes and do not measure static forces. Wang et al[18] introduced an optical fiber array to measure pressure and shear stresses from the light attenuation induced by the physical deformation of fibers. Although the optical fiber sensors have the advantages of being conformal and flexible, they are fragile and prone to damage during regular uses.

Besides the aforementioned disadvantages, the biggest limitation of most existing shear and pressure sensing technologies is the need of wire connections. In addition to the high installation and maintenance costs, it is difficult to measure the pressure and shear stress on moving parts or in harsh environments using cable connections. Our group has recently demonstrated a loop antenna for normal load sensing and a patch antenna for shear load sensing[19]. Even though, these antenna sensors can be wirelessly interrogated, these two types of antenna sensors have to be stacked on top of

*huang@uta.edu; phone 1 817 272-0563; fax 1 817 272-5010; website: astl.uta.edu .

Sensors and Smart Structures Technologies for Civil, Mechanical, and Aerospace Systems 2015, edited by Jerome P. Lynch, Kon-Well Wang, Hoon Sohn, Proc. of SPIE Vol. 9435, 943533
 · doi: 10.1117/12.2084129

each other to measure the shear and pressure forces simultaneously.

The paper discusses a pressure and shear sensor based on the principle of microstrip antenna technology and electromagnetic interference. The sensor consists of a patch antenna and a U-shaped metallic reflector. In addition to providing compact size, low profile, high sensitivity, and fine spatial resolution, the proposed sensor can be wirelessly interrogated without needing a battery[20]. The design and fabrication of the sensor as well as its characterization to detect shear and pressure respectively are presented in detail.

2. PRINCIPLE OF OPERATION

A microstrip patch antenna consists of a radiation patch, a ground plane, and a dielectric substrate. An electromagnetic resonator that radiates at specific resonant frequencies is formed between the conductive radiation patch and the ground plane. According to the transmission line model[21], the antenna resonant frequency f can be expressed as

$$f = \frac{c}{2\sqrt{\varepsilon_r} l_e}, \tag{1}$$

where ε_r is the substrate dielectric constant, c is the speed of light, and l_e is the electric length of the radiation patch. The fringe effects are ignored in Eq. (1) as long as the radiation dimensions satisfy the condition $l > w > l/2 >> h$. For a patch antenna with a rectangular radiation patch, the two fundamental resonant modes are the TM_{010} mode whose electric current flows along the length direction of the radiation patch and the TM_{001} mode whose electric current flows along the width direction of the radiation patch. When the resonant frequency of the TM_{010} mode is calculated, the electrical length l_e is the physical length of the radiation patch. The resonant frequency of the TM_{001} mode can be calculated by simply substituting l_e with the physical width of the radiation patch w.

The shear and pressure sensor is designed based on the electromagnetic interference between a microstrip patch antenna and a reflector placed at a distance on top of the patch antenna. The lateral alignment of the antenna radiation patch and the reflector is shown in Figure 1. The reflector has a U-shaped metallic pattern that covers three edges of the radiation patch. Since the reflector is placed on top of the patch antenna, the electromagnetic wave radiated by the patch antenna will be reflected by the reflector and interfere with the electromagnetic field of the radiation patch, which results in the changes of the antenna resonant frequencies. This resonant frequency changes are related to the lateral and vertical positions of the reflector. Since a shear force will change the lateral position of the reflector while a normal pressure will reduces the distance between the metallic reflector and the radiation patch, the applied shear force and normal pressure can be detected by monitoring the antenna resonant frequencies.

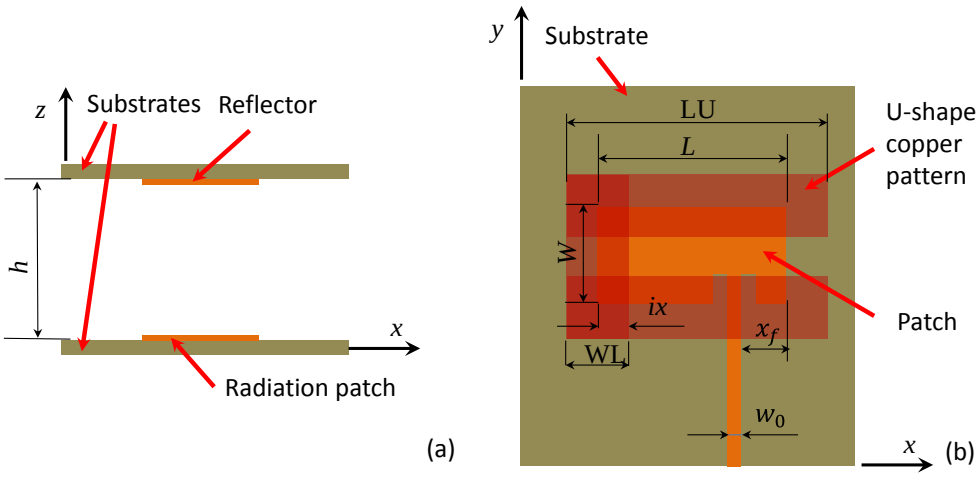

Figure 1. Schematic diagram of the shear and pressure sensor: (a) front view, and (b) top view.

3. ANTENNA SENSOR DESIGN, FABRICATION, AND TESTING

The design parameters of the shear and pressure sensor can be divided into two categories, i.e. the antenna design parameters and the reflector design parameters. As listed in Table 1, the antenna design parameters include the radiation patch dimensions L and W, the feedline width w_0, and the feedline position x_f. The radiation patch dimensions L and W determine the antenna resonant frequencies and their linear responses to shear and pressure deformations. Parameters w_0 and x_f affect the performance of the patch antenna such as the gain, the bandwidth, etc. The resonant frequencies of the patch antenna were designed to be 6.1 GHz (TM_{010} mode) and 6.85 GHz (TM_{001} mode), respectively. The reflector design parameters include the U-pattern geometric parameters such as WL, LU, WU, WS, the distance between the radiation patch and the reflector h, and the initial position of the reflector relative to the radiation patch ix along the x-direction. In order to ensure the electromagnetic interference between the radiation patch and the metallic reflector, h is suggested to be smaller than 5 mm for the operation frequency in the range of 3-8 GHz. The initial position ix affects the sensor performance such as linearity.

Table 1 Sensor Design Parameters

Patch Antenna	
Radiation patch length, L (mm)	12.75
Radiation patch width, W (mm)	11.25
Feed position, x_f (mm)	2.5
Feeding width, w_0 (mm)	0.7
U-shaped Reflector	
U-shape arm width, WL (mm)	10
U-shape length, LU (mm)	35
U-shape width, WU (mm)	25
U-shape slot width, WS (mm)	5
Initial position, ix (mm)	0
Initial height, h_0 (mm)	2.5

A dielectric laminate with copper claddings on both sides (4350b from Rogers Corp.) was selected for fabricating the dual-frequency patch antenna and the U-shape copper reflector. A chemical etching method was used to fabricate both the reflector and the patch antenna. The geometry of the radiation patch and the transmission line were first printed on a PCB image transfer film (Techniks Inc., PNPB20). The transfer film was ironed on the dielectric substrate to transfer the printed pattern to the copper surface of the laminate. Before the transferring process, the transfer film was aligned to make sure the edges of radiation patch were parallel to laminate edges. After protecting the ground plane surface of the laminate with a tape to prevent it from being etched, the laminate with the printed pattern was submerged in a ferric chloride solution for 15-20 minutes to remove the exposed copper. Once the copper was completely etched, the remaining solution was washed off and the plastic tape was removed. The laminate was rinsed thoroughly in acetone to remove the ink and allowed to dry. The procedure of fabricating the U-shaped reflector on a laminate is similar. The side without the pattern was not protected by the tape before etching so that the copper on one side of the laminate will be removed completely. Figure 2a and 2b show the fabricated patch antenna and the U-shape reflector, respectively.

The experiment setup to test the sensor's response to the lateral and vertical displacements of the reflector is shown in Figure 3. The patch antenna and the reflector were fixed on two translation stages whose positions can be controlled using two manual micrometers. The patch antenna was allowed to move along the x-direction only while the reflector was only allowed to move along the z-direction. To measure the S11 parameter of the patch antenna, the patch antenna was connected to a Vector Network Analyzer (VNA) via a SMA connector and a co-axial cable. The antenna resonant frequencies were measured as the frequencies at which the S11 curve has a local minimum. The lateral shear displacement x was introduced by translating the reflector along the x-direction at fixed vertical distances between the antenna radiation patch and the reflector, i.e. h = 3.5 mm, 3.25 mm, 3.0 mm, 2.75 mm, and 2.5 mm, respectively. At each height h, the S11 curves were collected at a shear displacement increment of 0.5 mm, starting at x = 0 mm (i.e. ix=0 as shown in Figure 1b) and stopping at x = 4 mm. In total, 45 sets of S11 curves were obtained.

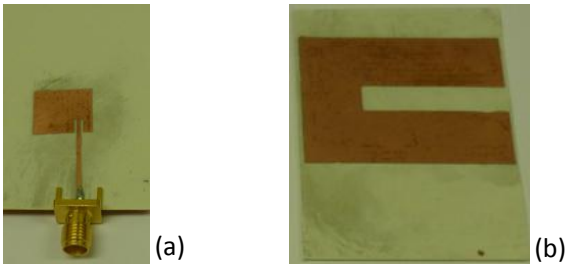

Figure 2. Fabricated (a) patch antenna, and (b) U-shaped reflector.

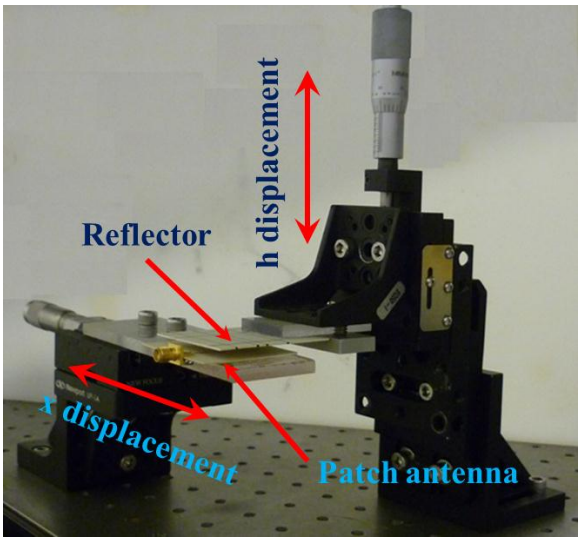

Figure 3. Experimental setup for sensor characterization.

4. NUMERICAL SIMULATION

A finite element model was created in HFSS according to the experimental setup described above. In a sufficiently large domain (500 mm X 500 mm X 200 mm), an electromagnetic system consists of the patch antenna, the air gap, the reflector, the ground plane, and two laminates was created. Since the interference have higher order effects on the electromagnetic field, a denser mesh strategy has to be applied to capture the resulted frequency shifts accurately. In order to achieve sufficiently accurate simulation results within an acceptable time, we ran a set of simulations with decreasing element sizes to ensure that the results have converged. Based on these convergence studies, an optimal configuration was selected according to the time consumption. The mesh configurations of the metallic parts and the air gap we adopted are shown in Figure 4. The maximum lengths of elements are 1 mm, 0.2 mm, and 2 mm for the copper U-pattern, the radiation patch, and the air gap, respectively, as depicted by Figure 4a, 4b, and 4c, respectively. The parametric study was carried out with respect to the two shear and normal displacements, i.e. the vertical distance between the reflector and the radiation patch *h* and the lateral shear displacement *x*. The vertical distance *h* was varied from 2.5 mm to 3.5 mm, with increments of 0.25 mm. The shear distance *x* was increased from 0 mm to 4 mm, with increments of 0.5 mm. The antenna return loss, i.e. the S11 curve, was calculated for each combination of these two parameters.

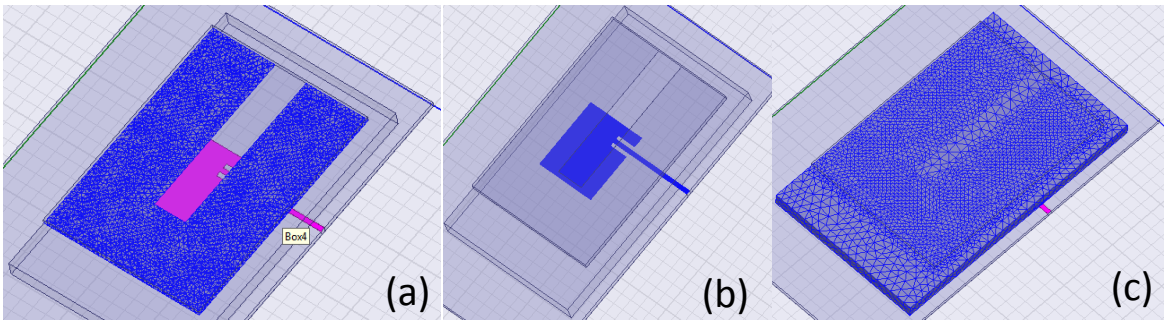

Figure 4. HFSS meshing of: (a) reflector; (b) radiation patch; and (c) air gap.

5. RESULTS AND DISCUSSIONS

5.1 Simulation Results

The simulated antenna resonant frequency changes as functions of the lateral displacement x and vertical displacement h are given in Figure 5. In Figure 5a and 5b, the f_{010} and f_{001} frequencies are plotted versus the vertical distance h for fixed x values. For a given x, the f_{010} frequency decreases linearly with h while the f_{001} frequency increased linearly. The slope of the h- f_{010} relationship appears to be independent of the lateral distance x. However, the slope of the h-f_{001} relationship decreases with the increase of x. When x is larger than 3 mm, the f_{001} frequency is insensitive to the change of distance h. Figure 5c and 5d plot the f_{010} and f_{001} frequencies as a function of x for fixed h values. As shown in Figure 5c, the f_{010} frequency does not change much with x when x is less than 1.5 mm. However, an approximately linear decrease of the f_{010} frequency can be observed when x is larger than 1.5 mm. The curves shown in Figure 5c are almost parallel, indicating that the vertical distance h does not have a strong influence on the slope of the x-f_{010} relationship. Figure 5d shows that the f_{001} resonant frequency increases with x. The curves in Figure 5d converges for x values that are larger than 3.0 mm.

5.2 Experimental Results

The changes of the antenna resonant frequencies under different shear and compression displacements, measured using the experimental setup shown in Figure 3, are shown in Figure 6. Similar to the simulation predictions, the resonant frequency change of each antenna mode is linear with respect to the compression and shear displacements, i.e., h and x. It is worth noting that the curves shown in Figure 6c show that the f_{010} frequency is sensitive to x changes even when x is less than 1.5 mm. This discrepancy may be due to the initial position of the reflector, which was controlled manually and may not match exactly with the simulation model.

5.3 Data processing

Selecting the parameter ranges that have linear relationships between the antenna resonant frequencies and the shear and normal displacements, we formulate the linear relationships using two equations containing bilinear terms, i.e.

$$f_{010} = a_{010}xh + b_{010}x + c_{010}h + d_{010}, \tag{2}$$

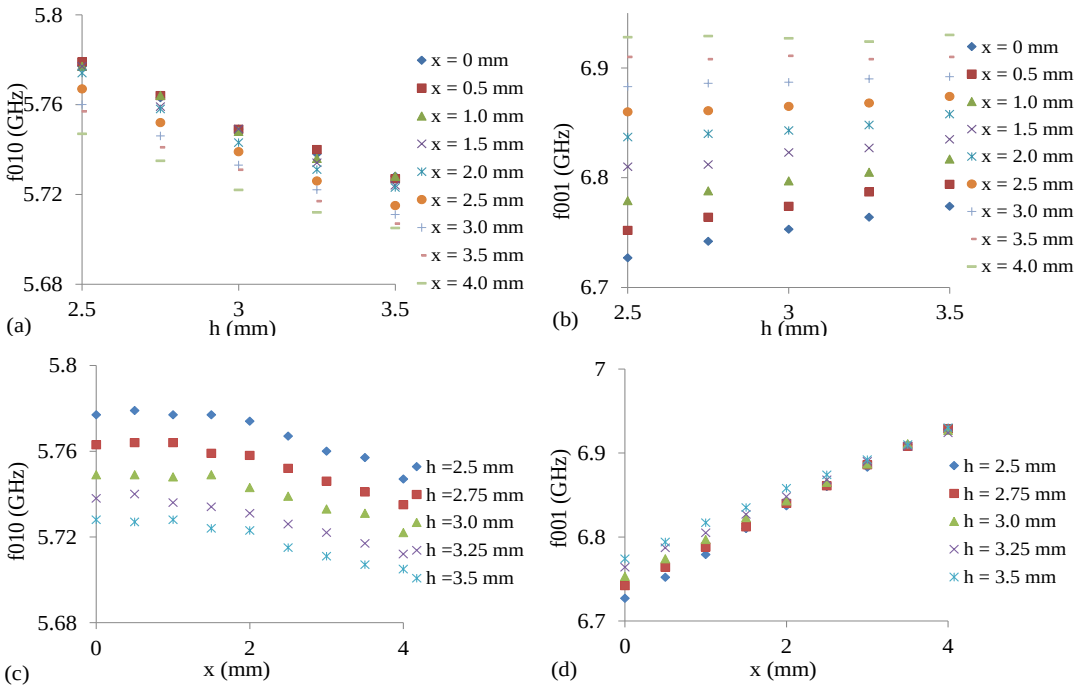

Figure 5 Simulation predictions – effects of shear and normal displacements on the antenna resonant frequencies: (a) f_{010}-h relationship at fixed x values; (b) f_{001}- h relationship at fixed x values; (c) f_{010}- x relationship at fixed h values; and (d) f_{001}- x relationship at fixed h values.

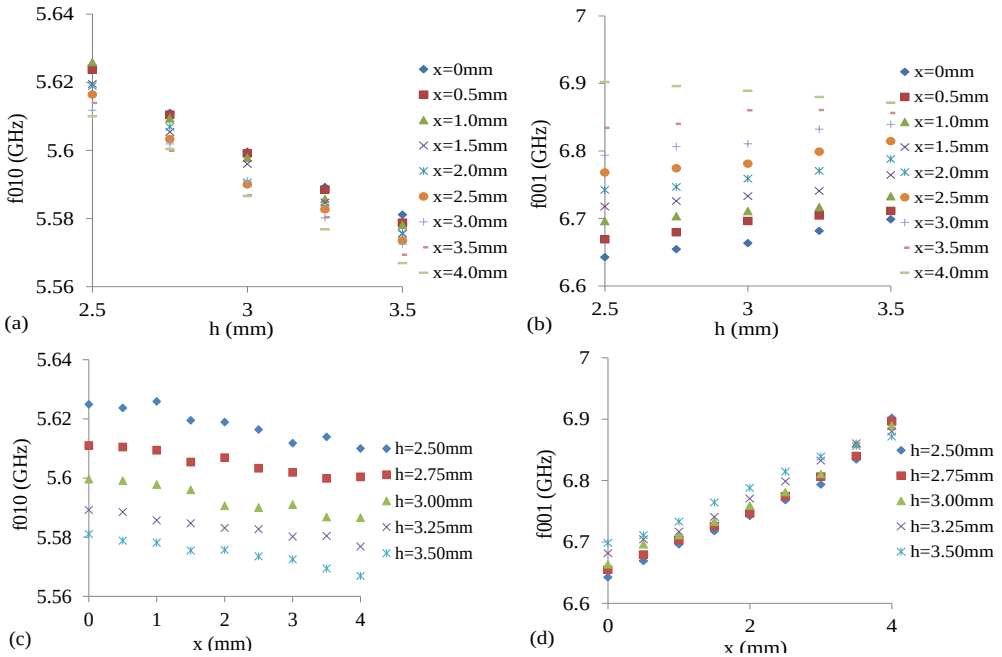

Figure 6 Experimental data – effects of shear and normal displacements on the antenna resonant frequencies: (a) f_{010}- h relationship at fixed x values; (b) f_{001}- h relationship at fixed x values; (c) f_{010}- x relationship at fixed h values; and (d) f_{001}- x relationship at fixed h values.

$$f_{001} = a_{001}xh + b_{001}x + c_{001}h + d_{001}, \tag{3}$$

where a_{0ij}, b_{0ij}, c_{0ij}, d_{0ij} are constants that can be obtained by curve fitting the experimental measurements using the least square (LSQ) method and their values are given in Table 2. Based on Table 2, we discovered that a_{010} is much smaller than the other three constants, which means that the coupling of the shear and normal displacements is very small. If this term can be neglected, equations (2) can be expressed as

$$x = \left(f_{010} - d_{010} - c_{010}h\right)/b_{010} \tag{4}$$

Substituting equation (4) into (3) results in a second order polynomial equation, i.e.

$$f_{001} = a_{001}\left(f_{010} - d_{010} - c_{010}h\right)h/b_{010} + b_{001}\left(f_{010} - d_{010} - c_{010}h\right)/b_{010} + c_{001}h + d_{001} \tag{5}$$

Therefore, the normal displacement h can be calculated from the two resonant frequencies and the constant values by solving equation (5). Once the compression displacement h is known, the shear displacement x can be calculated from equation (4).

Table 2 List of constants obtained from curve fitting of the experimental results.

TM010 mode									
a_{010}		b_{010}		c_{010}		d_{010}		statistics	
value	Standard error	value	Standard error	value	Standard error	value	Standard error	Reduced χ^2	Adjusted R^2
6.48E-04	6.14E-04	-0.00531	0.00185	-0.04505	0.00146	5.73685	0.00441	3.53E-06	0.98679
TM001 mode									
a_{001}		b_{001}		c_{001}		d_{001}		statistics	
value	Standard error	value	Standard error	value	Standard error	value	Standard error	Reduced χ^2	Adjusted R^2
-0.01241	0.0034	0.091	0.01029	0.05949	0.00811	6.48189	0.02448	1.09E-04	0.97916

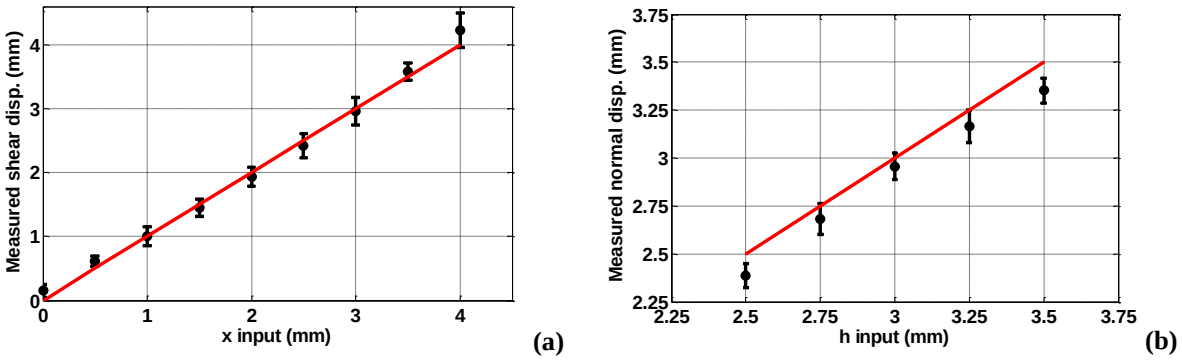

Figure 7. Measured displacements and their variances: (a) shear displacement *x*, and (b) normal displacement *h*.

As mentioned before, the antenna resonance frequencies were measured under combinations of nine *x* values and five *h* values. Figure 7 shows the shear and compression displacements inversely determined from the measured resonant frequencies and the corresponding measurement variances. The black dots represent the mean of the measured displacements, which is averaged over the measurements obtained at the same input levels. The error bars are symmetric about the mean value and their lengths were set as twice of the measurement variance. The red line represents the exact match between the measured and the input displacements, i.e. the 45° line. As shown in Figure 7(a), the shear displacements determined from the measured antenna resonant frequencies matched well with the actual shear inputs and the measurement variations are less than 0.25 mm. Even though the measured normal displacements appeared to have a slight offset from the actual displacements, the measurement variations are again less than 0.25 mm. Therefore, we can conclude that the presented antenna sensor can measure shear and normal displacement simultaneously.

6. CONCLUSIONS

A sensor consists of a microstrip patch antenna and a metallic reflector is presented in this paper for simultaneous measurement of shear and normal displacements. Due to the electromagnetic interference, the position of the metallic reflector relative to the radiation patch will shift the resonant frequencies of the patch antenna. Both the numerical simulation results and the experimental measurement indicate the antenna resonant frequencies are linearly proportional to the vertical and lateral displacements of the reflector. We successfully demonstrated that the shear and normal displacements can be inversely determined from the measured antenna resonant frequencies within an accuracy of less than 0.25 mm.

ACKNOWLEDGEMENT

This project is partially supported by the National Science Foundation under Grant CMMI-08460746 and the DOD Congress Directed Medical Research Program (CDMRP) under grant W81WXWH-14-1-0502.

REFERENCES

[1] Garrow, A. P., VanSchie, C. H. M. and Boulton, A. J. M., "Efficacy of multilayered hosiery in reducing in-shoe plantar foot pressure in high-risk patients with diabetes", Diabetes Care, 28, 2001-2006 (2005).
[2] Karkia, S., Lekkalaa, J., Kuokkanenb, H., and Halttunena, J., "Development of a piezoelectric polymer film sensor for plantar normal and shear stress measurements", Sensors and Actuators, 154, 57-64 (2009).
[3] Lord, M. and Hosein, R., "A study of in-shoe plantar shear in patients with diabetic neuropathy", Clinical Biomechanics, 15, 278-283 (2000).
[4] Davis, B. L., Perry, J. E., Neth, D. C. and Waters, K. C., "A device for simultaneous measurement of pressure and shear force distribution on the plantar surface of the foot", Journal of Applied Biomechanics, 14, 93-104 (1998).

[5] Jiang FK, Lee GB, Tai YC, Ho CM. "A flexible micromachine-based shear-stress sensor array and its application to separation-point detection". Sens. Actuat. A-Phys., 79:194–203 (2000).
[6] Ascari L, Corradi P, Beccai L, Laschi C. "A miniaturized and flexible optoelectronic sensing system for tactile skin". J. Micromechanic. Microengineer. 17:2288–2298,(2007).
[7] Hwang ES, Seo JH, Kim YJ. "A polymer-based flexible tactile sensor for both normal and shear load detections and its application for robotics". J. Microelectromechanical. Syst. 16:556–563, (2007).
[8] Ohka, M.; Kobayashi, H.; Mitsuya, Y., "Sensing characteristics of an optical three-axis tactile sensor mounted on a multi-fingered robotic hand". IEEE Int. Conf. Intell. Robots Syst. 493-498, (2005).
[9] Tappin, J.W., Pollard, J., Beckett, E.A., "Method of measuring 'shearing' forces on the sole of the foot". Clin. Phys. Physiol. Meas. 1, 83 – 85, (1980).
[10] Lord, M., Hosein, R.,Williams, R.B., "Method for in-shoe shear stress measurement". J. Biomed. Eng. 14, 181 – 186, (1992).
[11] Laing, P., Deogan, H., Cogley, D., Crerand, S., Hammond, P., Klenerman, L., "The development of the low profile Liverpool shear transducer". Clin. Phys. Physiol. Meas. 13, 115 – 124, (1992).
[12] Chen, W.M., Vee-Sin Lee, P., Park, S.B., Lee, S.J., Phyau Wui Shim, V., Lee, T., "A novel gait platform to measure isolated plantar metatarsal forces during walking". J. Biomech. 43, 2017 – 2021, (2010).
[13] Christ, P., Gender, M., Seitz, P., "A 3-D pressure distribution measurement platform with 8 × 8 sensors for simultaneous measurement of vertical and horizontal forces". VI Emed Scientific Meeting, (1998).
[14] Lei, K.F., Lee, K.F., Li, C.Y., "Analysis of the flexible PDMS capacitive microsensor for the 3-axis force measurement". Micro Nanosyst. 4, 208 – 213, (2012).
[15] Dobrzynska, J.A., Gijs, M.A.M., "Polymer-based flexible capacitive sensor for threeaxial force measurements". J. Micromech. Microeng. 23, (2013).
[16] Kärki, S., Lekkala, J., Kuokkanen, H., Halttunen, J., "Development of a piezoelectric polymer film sensor for plantar normal and shear stress measurements". Sensors Actuators A Phys. 154, 57 – 64, (2009).
[17] Koulaxouzidis, A.V., Holmes, M.J., Roberts, C.V., Handerek, V.A., "A shear and vertical stress sensor for physiological measurements using fibre Bragg gratings". Int. Conf. Eng. Med. Biol. Soc. 55 – 58, (2000).
[18] Wang, W.C., Ledoux, W.R., Sangeorzan, B.J., Reinhall, P.G., "A shear and plantar pressure sensor based on fibre-optic bend loss". J. Rehabil. Res. Dev. 42, 315 – 326, (2005).
[19] Mohammad, I. and Huang, H., "Shear sensing based on a microstrip patch antenna," Measurement Science and Technology, 23, 105705, (2012).
[20] Deshmukh, S., Mohammad, I., Xu, X. and Huang, H., "Unpowered antenna sensor for crack detection and measurement", Proc. SPIE 7647, 764742 (2010).
[21] Balansis C B [Antenna Theory: Analysis and Design], John Wiley & Sons, Inc, Hoboken, New Jersey, (2005).